1 *Supplementary Material for*

2 **"Observation-Constrained Kinetic Modelling of Isoprene SOA Formation in the**

3 **Atmosphere"**

4 Chuanyang Shen[1], Xiaoyan Yang[2], Joel Thornton[3], John Shilling[4], Chenyang Bi[5], Gabriel

5 Isaacman-VanWertz[6], Haofei Zhang[1*]

6 [1]Department of Chemistry, University of California, Riverside, CA, USA

7 [2]Department of Environmental Sciences, University of California, Riverside, CA, USA

8 [3]Department of Atmospheric Sciences, University of Washington, Seattle, Washington, USA

9 [4]Atmospheric Sciences and Global Change Division, Pacific Northwest National Laboratory,

10 Richland, WA, USA

11 [5]Center for Aerosol and Cloud Chemistry, Aerodyne Research Inc., MA, USA

12 [6]Department of Civil and Environmental Engineering, Virginia Tech, Blacksburg, Virginia, USA

13

14 [*]Corresponding Author.

15 E-mail address: haofei.zhang@ucr.edu (H. Zhang).

16

17 This PDF file includes:

18 No. of pages: 37

19 No. of supplemental text: 2

20 No. of tables: 8

21 No. of figures: 18

22 **Text S1:**

23 **Reactive uptake**

24   The reactive uptake coefficient (for epoxides, lactone, and alkylnitrates) can be described

25 as the following equation:

26
$$\frac{1}{\gamma} = \frac{r_p \omega}{4 D_{gas}} + \frac{1}{\alpha} + \frac{1}{\Gamma_{aq}}$$

27 The α is 0.02; D_{gas} is 0.1cm^2 s^{-1}; Γ_{aq} is calculated from the following equation:

28
$$\Gamma_{aq} = \frac{4 \, VRTH_{aq} k_{aq}}{SA * \omega}$$

29 for IEPOX, the ω is 2.81×10^4 cm s^{-1}; for HMML, the ω is 2.69×10^8 cm s^{-1}; V is the total particle

30 volume; R is the Universal gas constant of 0.08205 L atm mol^{-1} K^{-1}; for IEPOX, H_{aq} is 1.3×10^8

31 M atm^{-1}; for HMML, H_{aq} is estimated from EPI as 3.76×10^4 M atm^{-1}. The k_{aq} is calculated as:

32
$$k_{aq} = \sum_{i=1}^{N} \sum_{j=1}^{M} k_{i,j} [nuc_i][acid_j]$$

33 [nuc] is the concentration of nucleophiles (M) and it can be either the water or sulfate, [acid] is

34 the concentration of acids (M). All these parameters can be modeled using the ISORROPIA II.

35 a_{H^+} is the proton activity, and the $k_{i,j}$ is shown in the Table S8. In the model, we assume that the

36 reactive uptake of all epoxides follows the same reaction kinetics, that means the k_{i,H^+} and

37 $k_{i,HSO4^-}$ are the same for IEPOX, MGA and other epoxides. But the H_{aq} values are different given

38 by the EPI estimation.

39   **Text S2:**

40   **The model setup for different chamber experiments**

41   **UNC-2010/2012:**

42   In UNC-2010/2012, a total of 23 experiments were performed at the University of North

43   Carolina 270 m^3 dual outdoor smog chamber under clear natural sunlight. Overall, the initial

44   NO$_x$/isoprene ratios varied from 0.06 to 0.53, with initial isoprene concentration ranging from 200

45   ppb to 1250 ppb. The concentrations of O$_3$, NO$_x$ and isoprene were measured from the chamber

46   and the experimental facility can be referred to in previous studies (Kamens et al., 2011; Zhang et

47   al., 2011; Zhang et al., 2013). The experimental conditions for all these 23 experiments are

48   summarized in Table S3. J values, temperature (T) and RH are derived from real-time

49   measurements. The simulation is run in gas mode, which means only the gas-phase reactions are

50   allowed.

51   **Kroll-2006:**

52   Kroll-2006 included 8 unseeded NO$_x$-free experiments and 6 seeded high-NO$_x$ experiments.

53   The initial isoprene concentration varied from 12.2 ppb to 90 ppb for NO$_x$-free experiments. The

54   initial NO$_x$/isoprene ratios spanned a wide range from 1 to 16.9 with initial isoprene concentration

55   around 45 ppb for high-NO$_x$ experiments. The input values are shown in Table S4. The chamber

56   RH in the meteorology field is 50%. The J$_{NO2}$, J$_{NO3NO}$, J$_{NO3NO2}$, and J$_{H2O2}$ are 0.0048, 2×10^{-4},

57   4.6×10^{-4} and 2.9×10^{-6} s^{-1}, respectively (Thornton et al., 2020). Other J values are calculated from

58   solar zenith angle (SZA=50) using MCM's solar zenith angle parameterization. The C* threshold

59   is set as 100 μg m^{-3}, which means that species with C* >100 μg m^{-3} are excluded from contributing

60   to SOA formation and species otherwise will go through gas-particle partitioning to form the SOA.

61   Since the SOA measurements in our simulated chamber studies have been corrected for losses of

62   particles to walls, the model simulation does not include particle wall loss. For the vapor wall loss,

63   it was treated based on Zhang et al. (2014). The threshold to invoke wall partitioning is 1×10^6 µg

64   m^{-3}; The equivalent absorbing organic mass concentration of the wall material is set as 1×10^4 µg

65   m^{-3}; and the timescale to mix vapors to wall surface is set as 2.5×10^{-4} s^{-1}.

PNNL-2018:

67   The initial concentrations include isoprene, H_2O_2, NO, NO_2. The input values are shown

68   in Table S4. The chamber RH in the meteorology field is 5%. The J_{NO2}, J_{NO3NO}, J_{NO3NO2}, and J_{H2O2}

69   are 0.006, 2×10^{-4}, 4.6×10^{-4} and 2.2×10^{-6} s^{-1}, respectively. Other J values are calculated from solar

70   zenith angle (SZA=50). The C* threshold is set as 100 µg m^{-3}. No particle wall loss is included in

71   the model simulation. A first-order rate coefficient for irreversible vapor wall loss of 1×10^{-4} s^{-1} is

72   applied in the model.

PNNL-2014:

74   The initial concentrations include isoprene, H_2O_2 and NO, which are shown in Table S4.

75   The initial NO_x/isoprene ratios were 0-3.8. The J_{NO2} and J_{H2O2} are 0.006 s^{-1} and 2.5×10^{-6} s^{-1},

76   respectively. SZA is set to 50 and is used to calculate other J values. The experiments were

77   conducted in the continuous-flow steady-state mode in which reacts were continuously injected

78   into the chamber and the total flow into and out of the chamber is balanced, so the dilution factor

79   is set to 5.6×10^{-5} s^{-1} and continuous injections of isoprene, H_2O_2 and NO into the chamber are

80   included in the model. The C* threshold is set as 100 µgm^{-3}. Wall loss rate is set as 6×10^{-5} s^{-1}. A

81   first-order rate coefficient for irreversible vapor wall loss of 1×10^{-4} s^{-1} is applied in the model

82   (Thornton et al., 2020).

Schwantes-2019:

84   The initial concentrations include isoprene, CHO_3NO, NO, NO_2. The input values are

85   shown in Table S5. The initial NO_x/isoprene ratios were 8.7-13.2. The J_{NO2} is set as 4×10^{-4} s^{-1} and

86   the other J values are calculated from solar zenith angle (SZA=84.525), which can best fit the J_{NO2}.

87   The C* threshold is set as 100 µg m^{-3}. The model simulation doesn't include particle wall loss.

88   The threshold to invoke wall partitioning is 1×10^6 µg m^{-3}; The equivalent absorbing organic mass

89   concentration of the wall material is set as 1×10^4 µg m^{-3}; and the timescale to mix vapors to wall

90   surface is set as 2.5×10^{-4} s^{-1}.

91 **Ng-2008:**

92   Ng-2008 were performed in the dark at room temperature and under dry conditions

93   (RH<10%) using N_2O_5 as a source of NO_3 radicals. The initial isoprene concentration was 18.4-

94   101.6 ppb and seed aerosols are introduced into the chamber for most experiments. The initial

95   concentrations include isoprene and N_2O_5, as shown in Table S6. For these nighttime oxidation

96   simulations, the SZA is set as 90. For the vapor wall loss, the threshold to invoke wall partitioning

97   is 1×10^6 µg m^{-3}; The equivalent absorbing organic mass concentration of the wall material is set

98   as 1×10^4 µg m^{-3}; and the timescale to mix vapors to wall surface is set as 2.5×10^{-4} s^{-1}. No particle

99   wall loss is included in the model simulation.

100 **Schwantes-2015:**

101   Only the Experiment 8 in the reference is simulated here. The initial concentrations include

102   isoprene (24 ppb), NO_2 (100 ppb), HCHO (4 ppm) and O_3 (49 ppb). The SZA is set as 90 and all

103   the J values are 0, corresponding to nighttime oxidation.

104 **Carlsson-2023:**

105   The initial concentrations include: O_3, NO_2, isoprene, NO_3. The input values are shown in

106 Table S7. The temperature was set as 292 K. The SZA is set as 90, so all the J values are 0

107 corresponding to nighttime oxidation.

108

109   **Table S1.** Abbreviated names and descriptions of species appearing in the UCR-ISOP mechanism.

Abbreviated Name	Description
ISOP	Isoprene
MACR	Methacrolein
MVK	Methyl vinyl ketone
IEPOXOO	Peroxy radicals formed from IEPOX
NISOPO2	Lumped isoprene nitrooxy peroxy radicals
NIT1NO3OOA	Peroxy radicals formed from NIT1 oxidation (OH-abstraction of the aldehydic hydrogen atom)
NIT1OHOO	Peroxy radicals formed from isoprene 1-hydroxy nitrates
IMACO3	Peroxymethacryl radical (CH_2=C(CH_3)C(O)O_2)
MACROO	Lumped peroxy radicals produced from MACR oxidation (OH addition)
MVKOO	Lumped peroxy radicals produced from MVK oxidation (OH addition)
HC5	C5 hydroxy carbonyls
NIT1	Lumped isoprene carbonyl nitrates
NISOPOOH	Lumped isoprene hydroperoxyl nitrates
MACRN	Lumped MACR nitrate
MVKN	Lumped MVK nitrate
IMPAA	methacrylic peracid
IMAPAN	Methacryloyl peroxynitrate
IMAE	Methacrylic acid epoxide
IHMML	Hydroxymethyl-methyl-alpha-lactone
PYRUACD	Pyruvic acid
HPALD1	Lumped Z-hydroperoxy-methyl-butenals
HPALD2	Isoprene hydroperoxy aldehydes
ISOPOOH12	1,2-isoprene hydroxy hydroperoxides
ISOPOOH43	4,3-isoprene hydroxy hydroperoxides
ISOPOOHD	Delta isoprene hydroxy hydroperoxides
IEPOXB	1,4-dihydroxy epoxides
IEPOXD	3,4-dihydroxy epoxides
ISOP1OH2N	1,2-isoprene-derived hydroxy nitrate
ISOP3N4OH	4,3-isoprene-derived hydroxy nitrate
ISOPHND	Isoprene-derived hydroxy nitrates
IDH	Lumped isoprene dihydroxy products
IDC	Lumped isoprene dicarbonyls
IDN	Lumped isoprene dinitrates
ICHE	Lumped isoprene C5 oxidation products with 1 carbonyl, 1 hydroxy and 1 epoxide functional group
IDHPE	Lumped isoprene C5 oxidation products with 2 hydroxy, 1 hydroperoxide and 1 epoxide functional group
IDNE	Isoprene dinitrate epoxides
IHPE	Lumped isoprene hydroxy hydroperoxyl epoxides

IHNE	Lumped isoprene hydroxy nitrate epoxides
INPE	Lumped isoprene nitrate hydroperoxyl epoxides
ICNE	Lumped isoprene carbonyl nitrate epoxides
ICPE	Lumped isoprene carbonyl hydroperoxyl epoxides
IHNPE	Lumped isoprene hydroxy nitrate hydroperoxyl epoxides
ICPDH	Lumped isoprene C5 oxidation products with 1 carbonyl, 1 hydroperoxide and 2 hydroxy functional groups
IDHDP	Lumped isoprene dihydroxy dihydroperoxides
IDCHP	Lumped isoprene C5 oxidation products with 2 carbonyl, 1 hydroxy and 1 hydroperoxide functional group
ITHP	Lumped isoprene C5 oxidation products with 3 hydroxyl group and 1 hydroperoxide
ITHC	Lumped isoprene C5 oxidation products with 1 carbonyl and 3 hydroxyl functional groups
ICHNP	Lumped isoprene C5 oxidation products with 1 carbonyl, 1 hydroxy, and 1 epoxide functional group
IDHDN	Lumped isoprene C5 oxidation products with 2 hydroxy, 2 nitrate functional groups
IDHPN	Lumped isoprene C5 oxidation products with 2 hydroxy, 1 hydroperoxide and 1 nitrate functional group
IDHCN	Lumped isoprene C5 oxidation products with 2 hydroxy, 1 carbonyl and 1 nitrate functional group
ICHDN	Lumped isoprene C5 oxidation products with 1 carbonyl, 1 hydroxyl and 2 nitrate functional groups
ICDPN	Lumped isoprene C5 oxidation products with 1 carbonyl, 2 hydroperoxide and 1 nitrate functional group
IHPDN	Lumped isoprene C5 oxidation products with 1 hydroxy, 1 hydroperoxide and 2 nitrate functional groups
IHNDP	Lumped isoprene C5 oxidation products with 1 hydroxy, 1 nitrate and 2 hydroperoxide functional groups
IHNDC	Lumped isoprene C5 oxidation products with 1 hydroxy, 1 nitrate and 2 carbonyl functional groups
ITHN	Lumped isoprene C5 oxidation products with 3 hydroxy and 1 nitrate functional group
INPA	Lumped isoprene C5 oxidation products with 1 nitrate, 1 hydroperoxide and 1 carboxyl group
INCA	Lumped isoprene C5 oxidation products with 1 nitrate, 1 carbonyl and 1 carboxyl group
C4HP	Lumped hydroxy hydroperoxides produced from MACR and MVK oxidation
C4HC	Lumped hydroxy carbonyls produced from MACR and MVK oxidation
C4DH	Lumped dihydroxy oxidation products from MACR and MVK
C4ENOL	Lumped C4 enols from MACR and MVK

C4PN	Lumped hydroperoxyl nitrates produced from MACR and MVK oxidation
HPETHNL	(Hydroperoxy) ethanal
HPAC	Peroxylacetone
MGA	2-Methylglyceric acid produced from MACR oxidation (OH addition)
NMGA	2-Methylglyceric acid nitrate form produced from MACR oxidation (OH addition)
C10dimer	The dimer products formed from RO2 with RO2
ISOP1OHOO	Lumped isoprene 1-hydroxy peroxy radicals
ISOP4OHOO	Lumped isoprene 4-hydroxy peroxy radicals
ISOPOOHOO	Peroxy radicals formed from ISOPOOH oxidation (OH addition)
NIEPOXOO	Nitrated epoxy peroxy radicals
ISOPNOO	Peroxy radicals produced from INTR oxidation
IHDNOO	As above, but from IHDN
IHPNOO	As above, but from IHPN

110
111

Table S2. The C^* values under the temperature of 298K for the semi-volatile and low-volatile species in ISOP-UCR mechanism. One name in the ISOP-UCR mechanism may correspond to several isomers whose SMILES (simplified molecular-input line-entry system) and C^* values are listed in the table too. In the calculation of gas-particle partitioning, the lowest C^* value in the isomers is used.

Names	Formula	SMILES	C^*_Evaporation ($\mu g\ cm^{-3}$)	C^*_SIMPOL.1 ($\mu g\ cm^{-3}$)
IDHPE	$C_5H_{10}O_5$	CC(CO)(OO)C1OC1O	15.87	103.00
		CC1(C(CO)OO)[O]C1O	15.87	
IDHDP	$C_5H_{12}O_6$	CC(CO)(OO)C(CO)OO	0.03	2.03
		CC(CO)(OO)C(O)COO	0.14	
		CC(O)(COO)C(CO)OO	0.67	
ICPDH	$C_5H_{10}O_5$	OCC(C(C=O)(O)C)OO	244.11	24.00
		OOC(C=O)C(C)(O)CO	244.11	
		OCC(O)C(C)(OO)C=O	54.02	
		O=CC(O)C(C)(CO)OO	54.02	
		OCC(=O)C(C)(CO)OO	23.72	
IDHCN	$C_5H_9NO_6$	OCC(ON(=O)=O)C(C)(O)C=O	2599.78	51.43
		O=CC(C)(O)C(O)CON(=O)=O	9131.41	
		O=CC(O)C(C)(CO)ON(=O)=O	625.60	
		O=CC(O)C(C)(O)CON(=O)=O	9131.41	
		OCC(O)C(C)(C=O)ON(=O)=O	625.60	
		[O-][N+](=O)OC(C(CO)(O)C)C=O	2599.78	
IDCHP	$C_5H_8O_5$	CC(O)(C(=O)OO)C(=O)C	102097.15	8950.00
		OCC(C(=O)C)C(=O)OO	2454.80	
		OCC(OO)(C=O)C(=O)C	1045.76	418.00
		OCC(=O)C(C)(OO)C=O	3446.76	
ITHP	$C_5H_{12}O_5$	CC(O)(CO)C(CO)OO	2.34	3.33
		CC(CO)(OO)C(O)CO	0.49	
ITHC	$C_5H_{10}O_4$	CC(O)(CO)C(=O)CO	1461.84	93.60
		O=CC(CO)C(O)CO	24.46	38.70
IDHPN	$C_5H_{11}NO_7$	OCC(C)(OO)C(O)CON(=O)=O	1.77	4.29
		OCC(OO)C(C)(CO)ON(=O)=O	0.46	
		OOCC(O)C(C)(CO)ON(=O)=O	1.77	
		OCC(OO)C(C)(O)CON(=O)=O	8.00	
		OCC(ON(=O)=O)C(C)(CO)OO	0.46	
ICHNP	$C_5H_9NO_7$	OCC(ON(=O)=O)C(C)(OO)C=O	47.21	30.98
		OOC(C)(C=O)C(O)CON(=O)=O	165.74	
		OOC(C=O)C(C)(CO)ON(=O)=O	47.21	
		O=CC(O)C(C)(OO)CON(=O)=O	165.74	

		OCC(C(O[N+](=O)[O-])(C=O)C)OO	47.21	
		O=CC(C(OO)(CO)C)O[N+](=O)[O-]	47.21	
IDHDN	C$_5$H$_{10}$N$_2$O$_8$	OCC(ON(=O)=O)C(C)(CO)ON(=O)=O	5.62	8.83
		OCC(C)(ON(=O)=O)C(O)CON(=O)=O	19.74	
		OCC(ON(=O)=O)C(C)(O)CON(=O)=O	82.02	
ICHDN	C$_5$H$_8$N$_2$O$_8$	O=CC(ON(=O)=O)C(C)(CO)ON(=O)=O	492.21	64.04
		OCC(ON(=O)=O)C(C)(C=O)ON(=O)=O	492.21	
		O=CC(C)(ON(=O)=O)C(O)CON(=O)=O	1391.55	
		O=CC(ON(=O)=O)C(C)(O)CON(=O)=O	4786.72	
IHPDN	C$_5$H$_{10}$N$_2$O$_9$	CC(CO)(ON(=O)=O)C(COO)ON(=O)=O	1.46	5.24
		CC(COO)(ON(=O)=O)C(CO)ON(=O)=O	1.46	
		CC(COO)(ON(=O)=O)C(O)CON(=O)=O	5.14	
		CC(O)(CON(=O)=O)C(COO)ON(=O)=O	21.36	
IHNDP	C$_5$H$_{11}$NO$_8$	CC(CO)(OO)C(COO)ON(=O)=O	0.13	2.57
		CC(CO)(OO)C(CON(=O)=O)OO	0.13	
		CC(COO)(ON(=O)=O)C(CO)OO	0.13	
		CC(CON(=O)=O)(OO)C(CO)OO	0.13	
		CC(CO)(ON(=O)=O)C(COO)OO	0.13	
		CC(COO)(OO)C(CO)ON(=O)=O	0.13	
IHNDC	C$_5$H$_7$NO$_6$	O=CC(=O)C(C)(CO)ON(=O)=O	34628.29	896.43
		O=CC(O)C(C)(C=O)ON(=O)=O	50778.52	
		O=CC(=O)C(C)(O)CON(=O)=O	336740.22	
		O=CC(C(C=O)(O)C)O[N+](=O)[O-]	174659.59	
ITHN	C$_5$H$_{11}$NO$_6$	CC(O)(CO)C(CO)ON(=O)=O	29.08	7.11
		CC(CO)(ON(=O)=O)C(O)CO	6.44	
IHNPE	C$_5$H$_9$NO$_7$	O=N(=O)OCC1(COO)OC1CO	28.47	132.21
ICNE	C$_5$H$_7$NO$_5$	CC1(CON(=O)=O)OC1C=O	1282937.17	220289.06
INPE	C$_5$H$_9$NO$_6$	CC1(COO)OC1CON(=O)=O	12333.61	18569.88
IHNE	C$_5$H$_9$NO$_5$	CC1(CO)OC1CON(=O)=O	50430.41	30557.83
ICPE	C$_5$H$_8$O$_4$	CC1(COO)OC1C=O	364022.82	101000.00
ICHE	C$_5$H$_8$O$_3$	CC1(CO)OC1C=O	14117988.17	160000.00

IDNE	$C_5H_8N_2O_7$	CC1(CON(=O)=O)OC1CON(=O)=O	42133.98	38763.39
IHPE	$C_5H_{10}O_4$	CC1(COO)OC1CO	16317.00	13969.74
INPA	$C_5H_7NO_6$	CC(=CC(=O)OO)CON(=O)=O	40944.98	71687.98
INCA	$C_5H_7NO_5$	CC(=CC(=O)O)CON(=O)=O	4509.29	5389.39

118

119

Table S3. The initial conditions of UNC chamber experiments.

Run	[isoprene] (ppb)	[NO] (ppb)	[NO$_2$] (ppb)	[NO$_x$] (ppb)	[isoprene]/[NO$_x$]
20090701N	400	159.9	29.6	189.5	2.11
20090703N	400	183.1	26	209.1	1.91
20090703S	400	95.6	22.6	118.2	3.38
20100622N	1100	91.2	26.3	117.5	9.36
20100622S	1250	185.8	50.1	235.9	5.30
20100705N	410	93.8	5.3	99.1	4.14
20100904N	950	29.1	24.6	53.7	17.69
20100904S	800	104.4	30.3	134.7	5.94
20101015N	400	142	9	151	2.65
20101015S	430	138.3	0.1	138.4	3.11
20101021N	790	253.4	0.1	253.5	3.12
20101021S	800	252	0	252	3.17
20110630S	392	94.4	32.2	126.6	3.10
20120531S	950	209.5	36.3	245.8	3.86
20120603N	780	65.2	38.7	103.9	7.51
20120603S	590	66.6	38.7	105.3	5.60
20120608N	1000	73.7	29	102.7	9.74
20120608S	370	74.7	29.5	104.2	3.55
20120628S	200	68.8	31.5	100.3	1.99
20120630N	760	141.7	49	190.7	3.99
20120630S	680	141.4	49.6	191	3.56
20120705N	980	163	23.8	186.8	5.25
20120705S	410	162.6	25.9	188.5	2.18

120

121 **Table S4.** The initial conditions of Kroll-2006 and PNNL-2018 experiments.

Chamber	Run	[isoprene] (ppb)	[H_2O_2] (ppm)	[NO] (ppb)	[Seed] ($\mu m^3 cm^{-3}$)	T (°C)
Kroll-2006	1	90	3.5	0	N/A	25.4
	2	46.1	3.5	0	N/A	25.6
	3	23	3.5	0	N/A	26
	4	12.2	3.5	0	N/A	25.7
	5	63.6	3.5	0	N/A	26.7
	6	29.4	3.5	0	N/A	28.7
	7	47.8	3.5	0	N/A	26.6
	8	41.6	3.5	0	N/A	26.4
	9	46.7	3.5	242	4.6	28.3
	10	43.5	3.5	496	7.1	28.3
	11	42.7	3.5	98	6.4	28.1
	12	49.1	3.5	51	6.5	28.2
	13	42.7	3.5	337	4.8	28.3
	14	42	3.5	708	4.7	27.5
PNNL-2018	1	43.5	7.5	0	0.3	24
	2	65	7.5	0	0.3	24
	3	69	7.5	0	0.3	24
	4	56.5	7.5	0	0.3	24
	5	51	7.5	0	0.3	24
	6	57	7.5	0	0.3	24
	7	48	7.5	0	0.3	24
PNNL-2014	1	26	15	0	0.3	25.4
	2	26	10	0	0.3	25.4
	3	26	10	2	0.3	25.4
	4	26	10	5	0.3	25.4
	5	26	10	10	0.3	25.4
	6	26	10	20	0.3	25.4
	7	26	10	50	0.3	25.4

122

123

Table S5. The experimental conditions of Schwantes-2019 experiments.

Run	[isoprene] (ppb)	[NO] (ppb)	[NO$_2$] (ppb)	[CH$_3$ONO] (ppb)	[Seed] ($\mu m^3 cm^{-3}$)	T (°C)	RH (%)
1	59	585	6	118	0	25.6	5
2	58	526	20	117	54	26.4	5.6
3	57	519	17	117	183	25.9	7.5
4	58	518	18	116	337	26.4	7.9
5	55	506	20	117	159	12.8	16.4
6	56	541	16	118	152	32.4	5.9
7	40	527	18	117	197	25.9	8.1
8	60	519	20	118	109	25.5	44.7
9	55	489	20	119	166	25.6	78.1
10	58	516	17	111	85	25.8	5.1
11	56	490	17	115	264	25.8	5.2

124

125

Table S6. The experimental conditions of Ng-2008 experiments.

Run	[isoprene] (ppb)	$[N_2O_5]$ (ppb)	T (°C)	RH (%)	SOA Yield (%)
1	101.6	1000	21	5.1	23.8
2	30.2	1000	20	4.7	13.5
3	67.1	1000	21	5.4	20.8
4	51.7	1000	20	6	18.2
5	18.4	1000	21	5.7	4.3
6	21.8	1000	21	5.5	7.8
7	39.5	1000	20	5.5	7.1
8	42	1000	21	6.4	14.1

126

127

Table S7. The experimental conditions of Carlsson-2023.

Run	[isoprene] (ppb)	[NO$_3$] (ppt)	[NO$_2$] (ppb)	[O$_3$] (ppb)	T (K)
1	2.4	5	5	101	297
2	1.69	40	4.5	100	295
3	2.5	3.5	12	78	295
4	4.4	250	25	105	292

128

129   **Table S8.** The parameters in the calculation of reactive uptake of IEPOX.

Product species	Parent species	Nucleophile	$k_{i,H^+}[M^{-2}s^{-1}]$	$k_{i,HSO4^-}[M^{-2}s^{-1}]$
2-MT	IEPOX	Water	2×10^{-4}	1.3×10^{-5}
IEPOX- OS	IEPOX	Sulfate	2×10^{-4}	2.9×10^{-6}

130

131
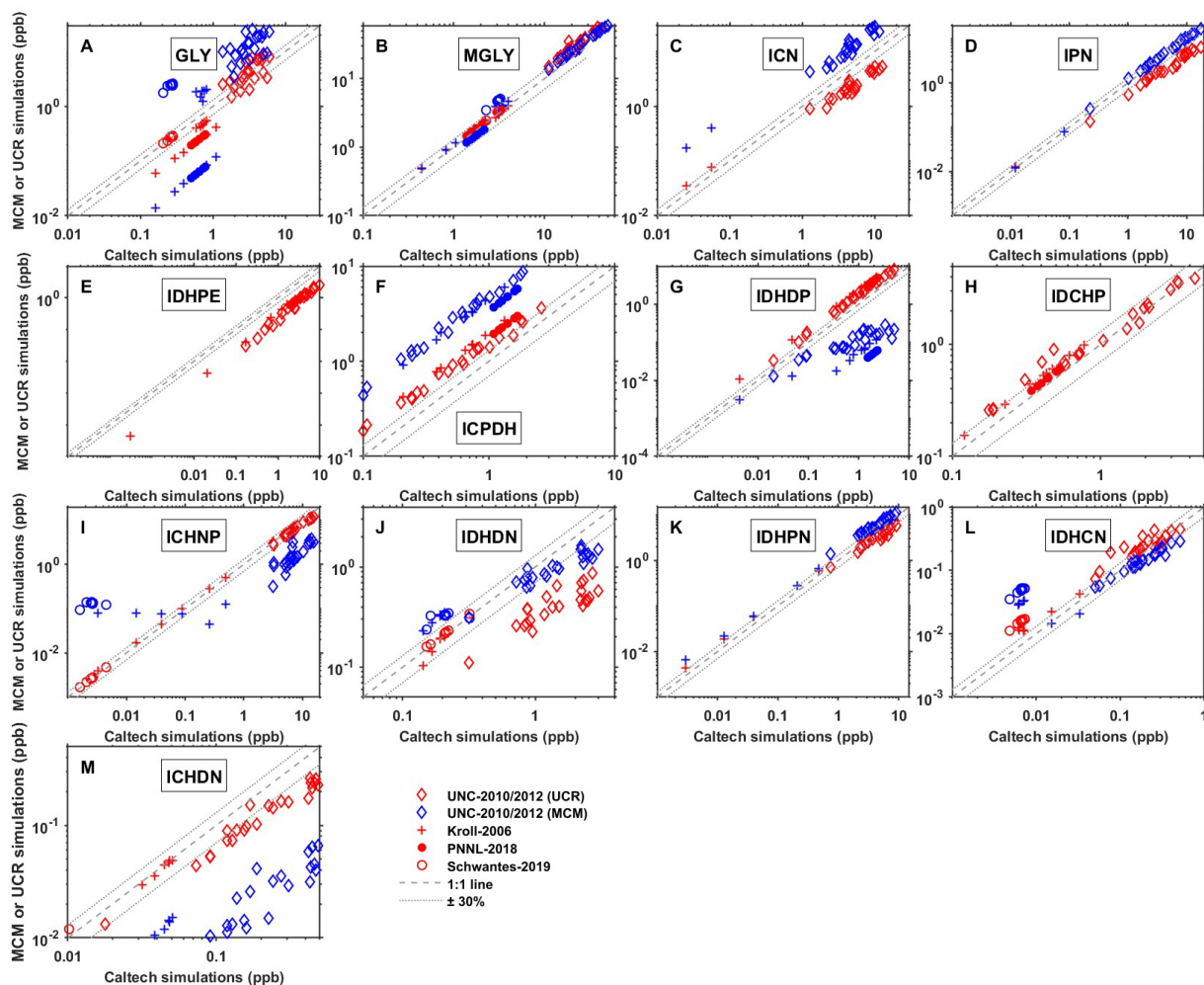
Figure S1. Comparison of simulated and measured species' maximum concentrations from different chemical mechanisms. The *x*-axis represents maximum concentrations from Caltech mechanism and y-axis represents values from UCR-ISOP (red markers) or MCM mechanism (blue markers). Different marker types represent different chamber studies.
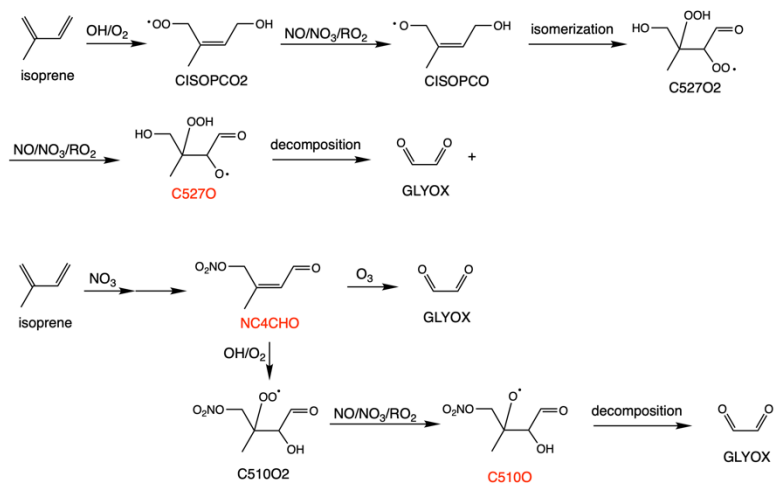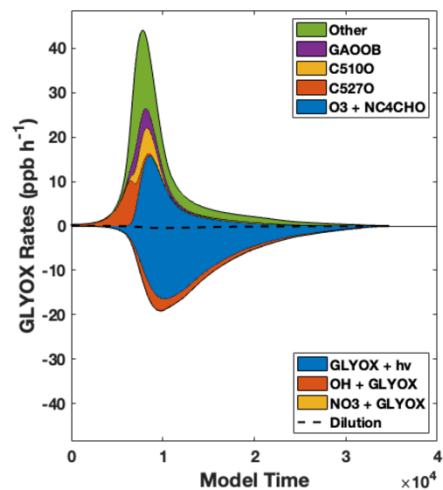
136

137 **Figure S2.** Left panel: major contributors to the formation and consumption of glyoxal (GLYOX)

138 in the MCM mechanism. Right panel: MCM pathways leading to glyoxal formation.

139
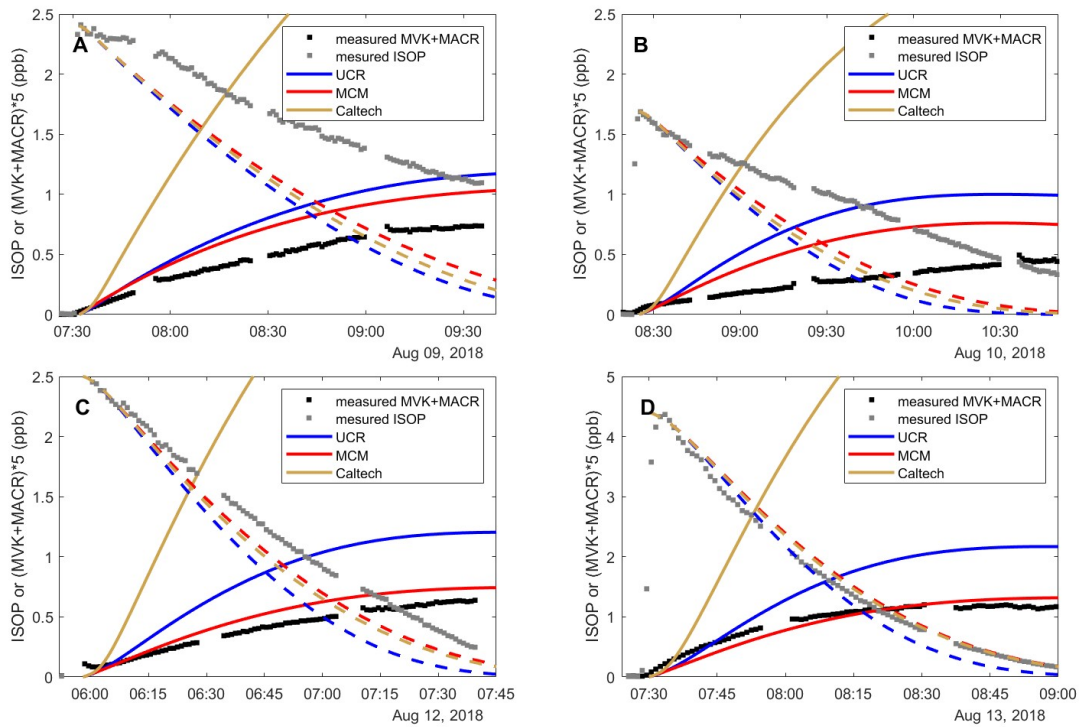
Figure S3. The simulation of Carlsson-2023 chamber study using different chemical mechanisms. The Caltech mechanism largely overpredict the concentration of MVK+MACR compared to measurements. The isoprene decays were overpredicted in (a)-(c) possibly due to the uncertainties in initial isoprene and NO_3 concentrations.
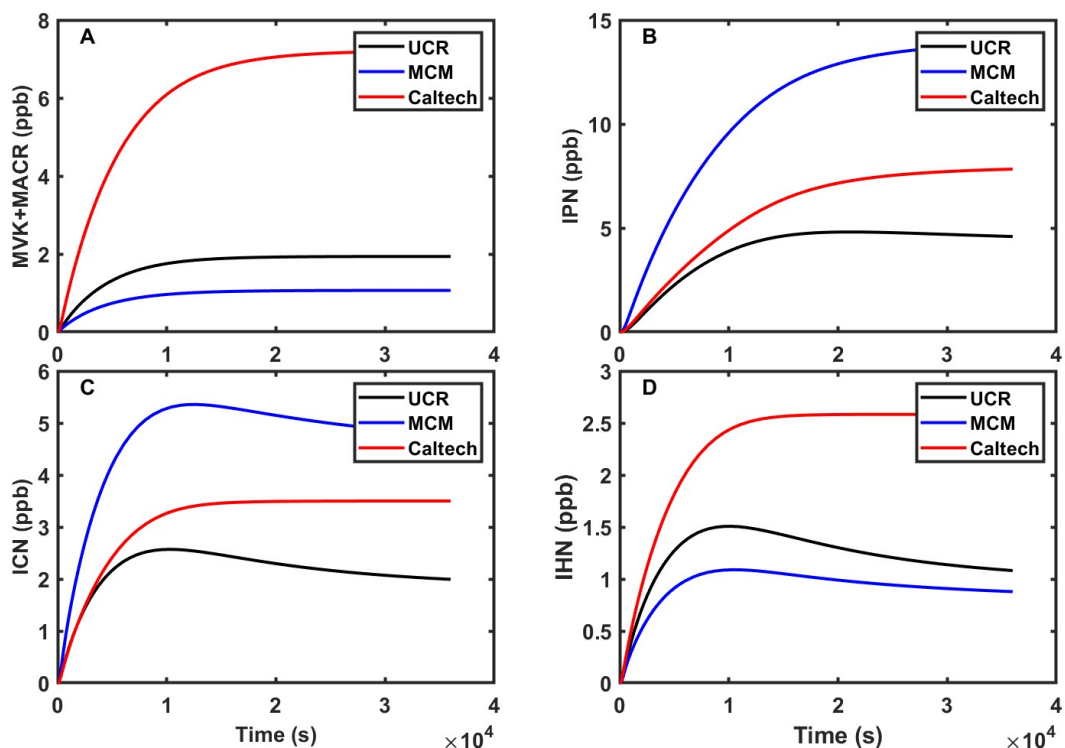
144
145 **Figure S4.** The simulation of Experiment 8 in Schwantes-2015 chamber study using different

146 chemical mechanisms. (a) is the comparison of MVK+MACR; (b) is the comparison of

147 hydroperoxide nitrates (IPN); (c) is the carbonyl nitrates (ICN) and (d) is the hydroxyl nitrates

148 (IHN). In comparison to the measurements (see Schwantes et al. (2015) Fig. 2), the simulated IPN

149 is slightly higher (5 ppb vs. 4 ppb); the simulated ICN is higher by a factor of ~2 (2 ppb vs. 1.2

150 ppb); and IHN is similar (~ 1 ppb). The later decreases in the UCR-ISOP and MCM mechanisms

151 are due to further oxidation, which is not included in the Caltech mechanism.

152
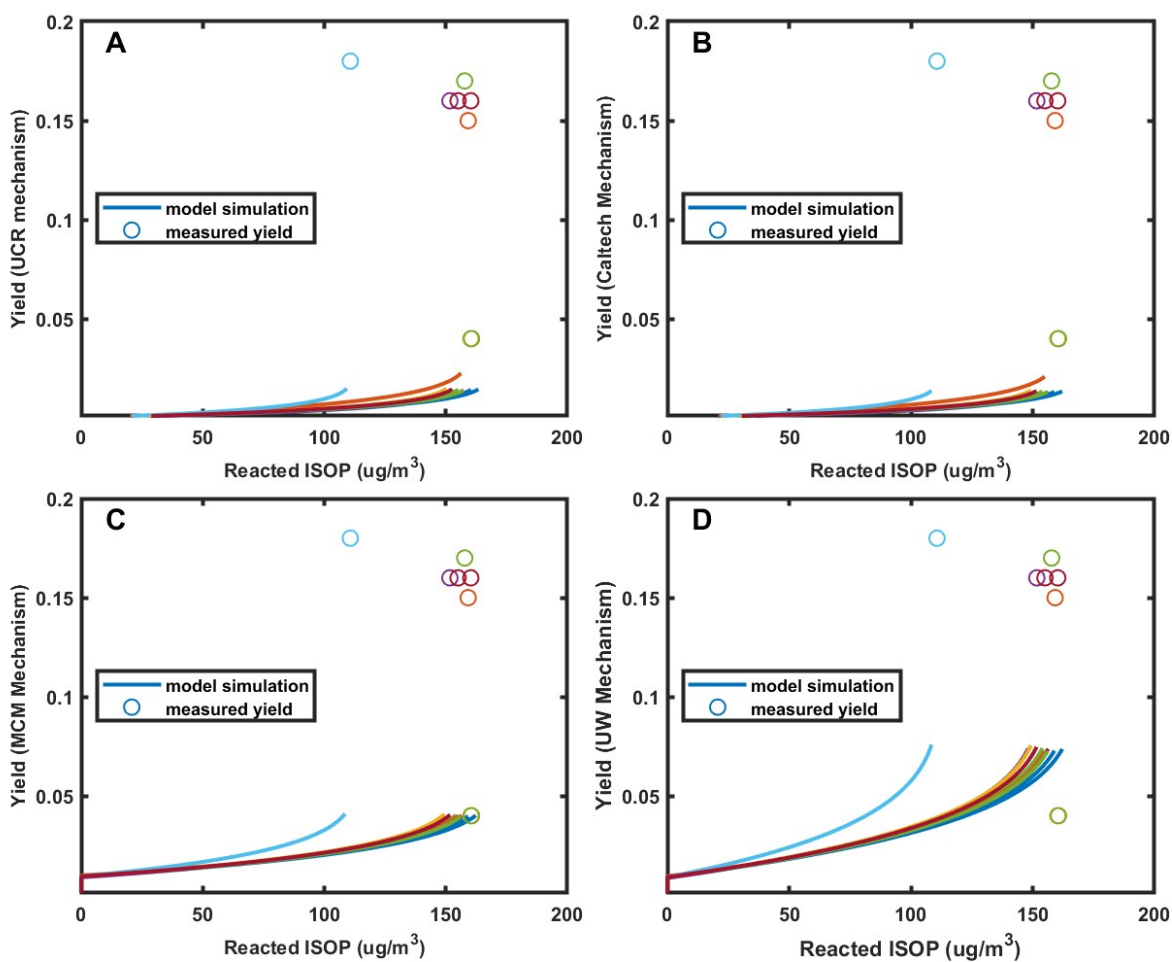
Figure S5. Model predicted isoprene SOA yield using different chemical mechanisms for Schwantes-2019 chamber study under high-NO$_x$ conditions. Different colors represent different experimental runs. Experimental conditions for each run can be found in Table S5. The yield is calculated from the modeled gas phase concentrations of IDHDN, IDHPN, IDHPN, ICHNP, IDHCN and ICHDN assuming they can entirely partition into particle phase.

158
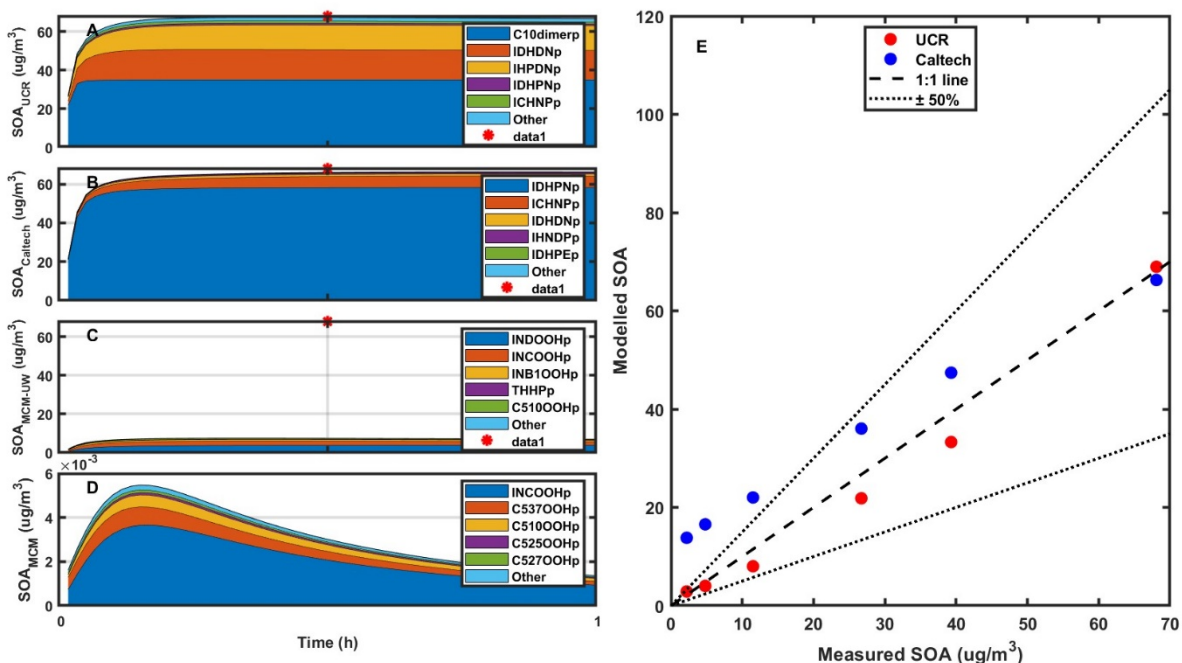
Figure S6. (a-d) The chemical constituents of modeled isoprene SOA in the Ng-2008 chamber study using different chemical mechanisms: (a) UCR-ISOP; (b) Caltech; (c) MCM-UW; and (d) MCM. In the MCM-UW mechanism, INDOOH, INCOOH and INB1OOH correspond to three isomers of IDHPN in UCR-ISOP mechanism; THHP correspond to the species with three -OH functional groups and one -OOH functional group. The species corresponding to the names in (c-d) can be found in MCM website (https://mcm.york.ac.uk/MCM). (e) The comparison of modeled SOA and measured SOA using UCR-ISOP and the Caltech mechanism.

166
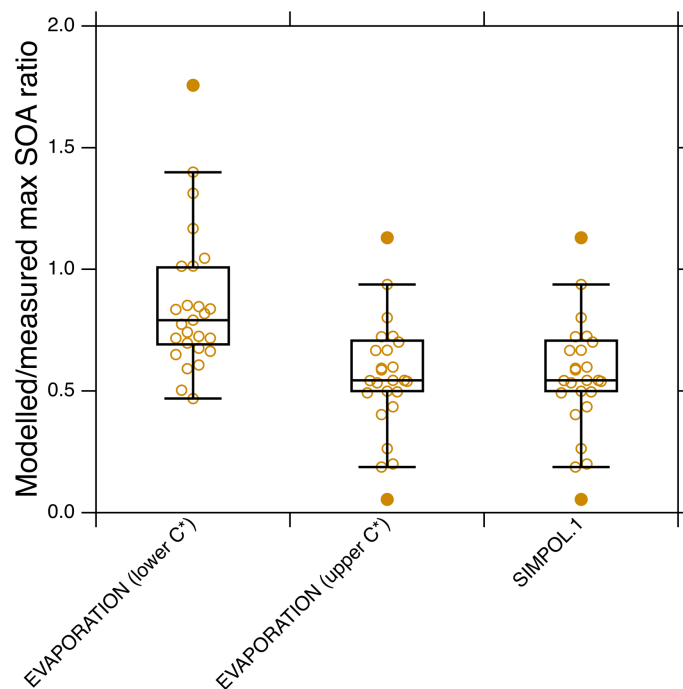
Figure S7. The distribution of modelled/measured SOA ratio using different vapor pressure estimation methods. The data used includes Kroll-2006, PNNL-2018, PNNL-2014 and Ng-2008 chamber experiments. For each box, the central horizontal line in the box indicates the median, and the bottom and top edges of the box indicate the 25th and 75th percentiles, respectively. The whiskers extend to the most extreme data points not considered outliers, and the outliers are plotted using the solid circle markers (other data points plotted using open circle markers).

173
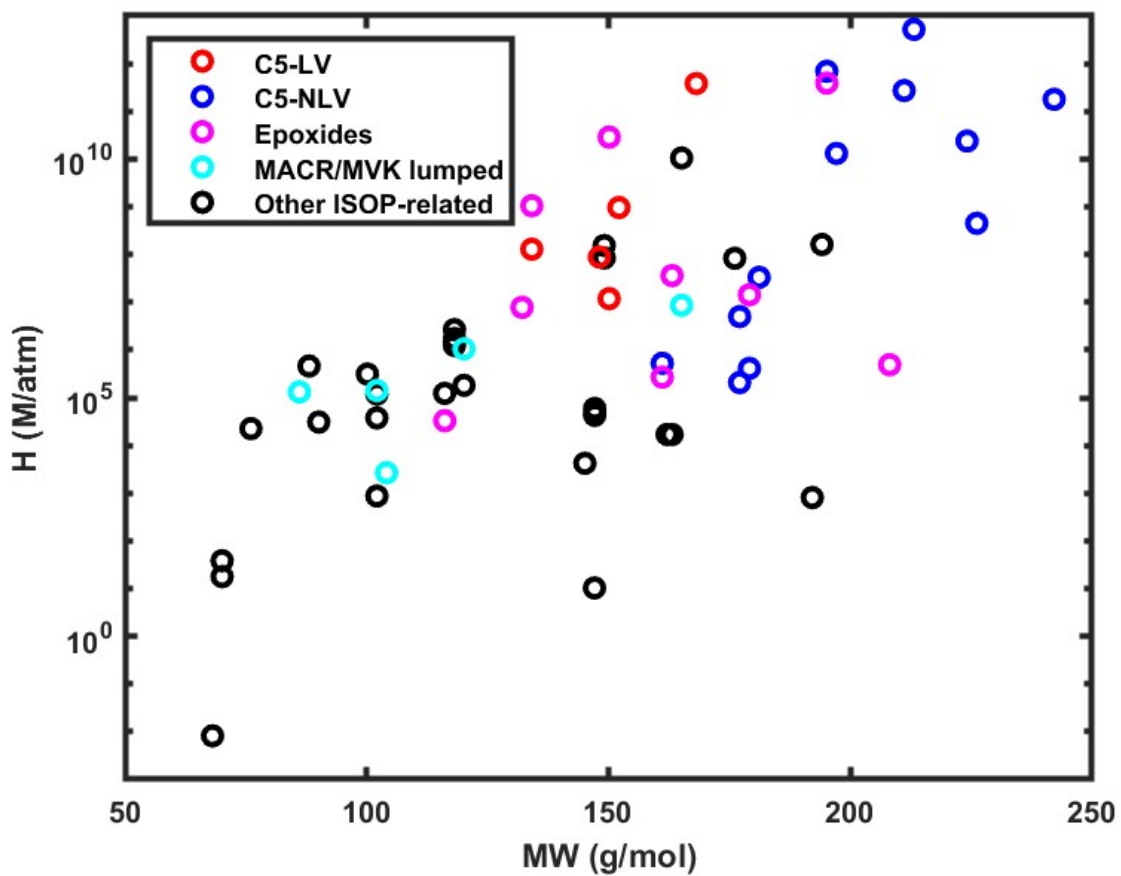
Figure S8. The distribution of Henry's law constants (H_{aq}) and molecular weight (MW) for isoprene oxidation products. Different colors represent different groups, e.g., the red open circles represent those five-carbon low-volatile species without nitrogen (C5-LV) and the blue open circles represent those five-carbon nitrogen-containing low-volatile species (C5-NLV).

178
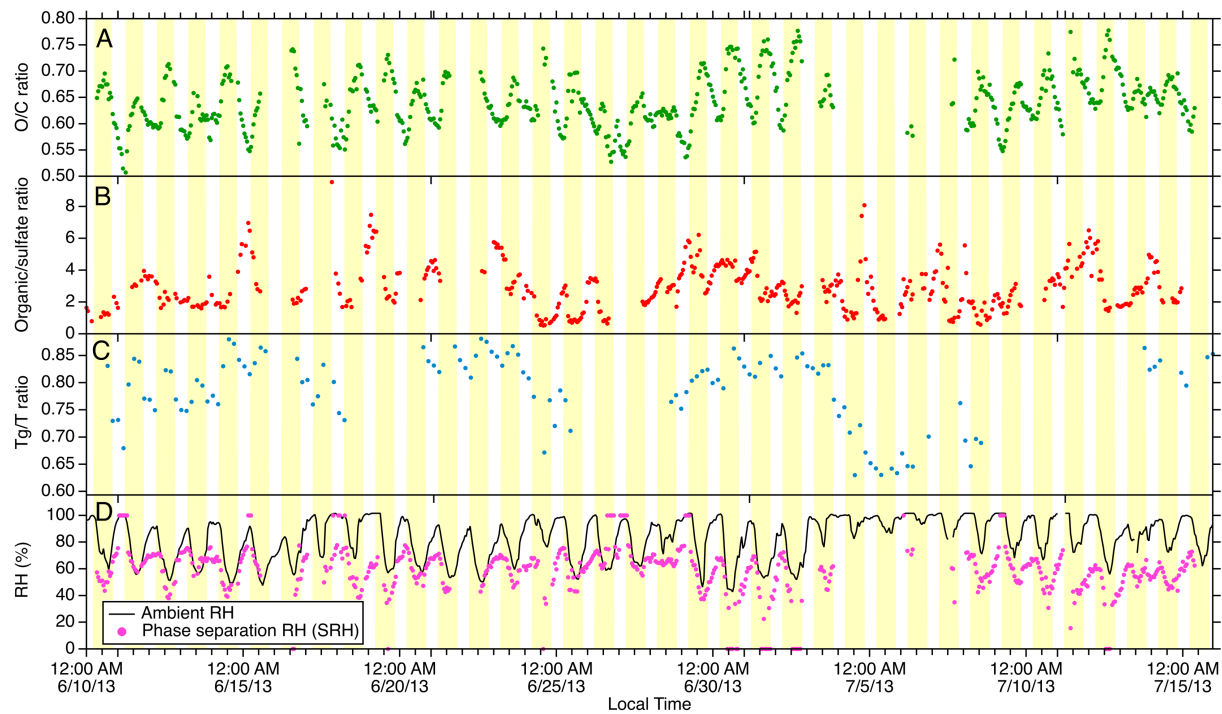
Figure S9. The time series of (A) measured O/C ratio, (B) organic aerosol/sulfate ratio, (C) glass

transition temperature (T_g) over ambient temperature (T) (Schmedding et al., 2020), and (D)

predicted phase separation RH (SRH) and ambient RH.

182
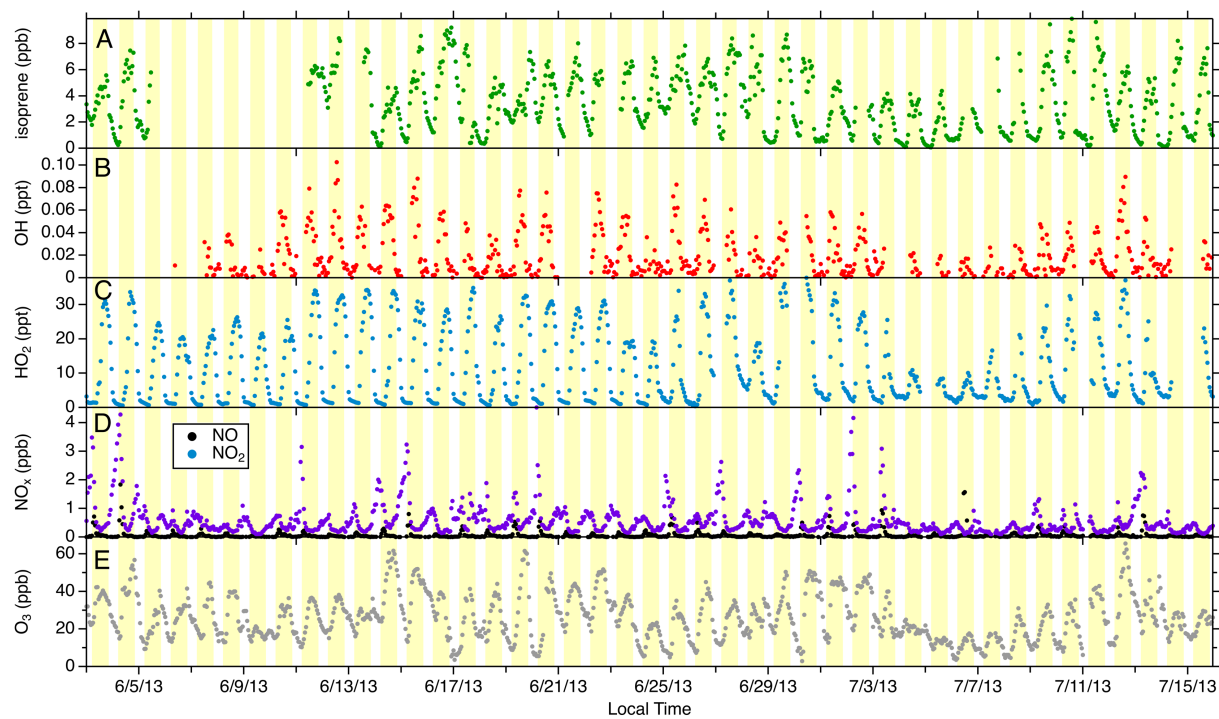
Figure S10. The time series of (A) isoprene, (B) OH, (C) HO_2, (D) NO and NO_2, and (E) O_3 during

the SOAS field campaign.

185
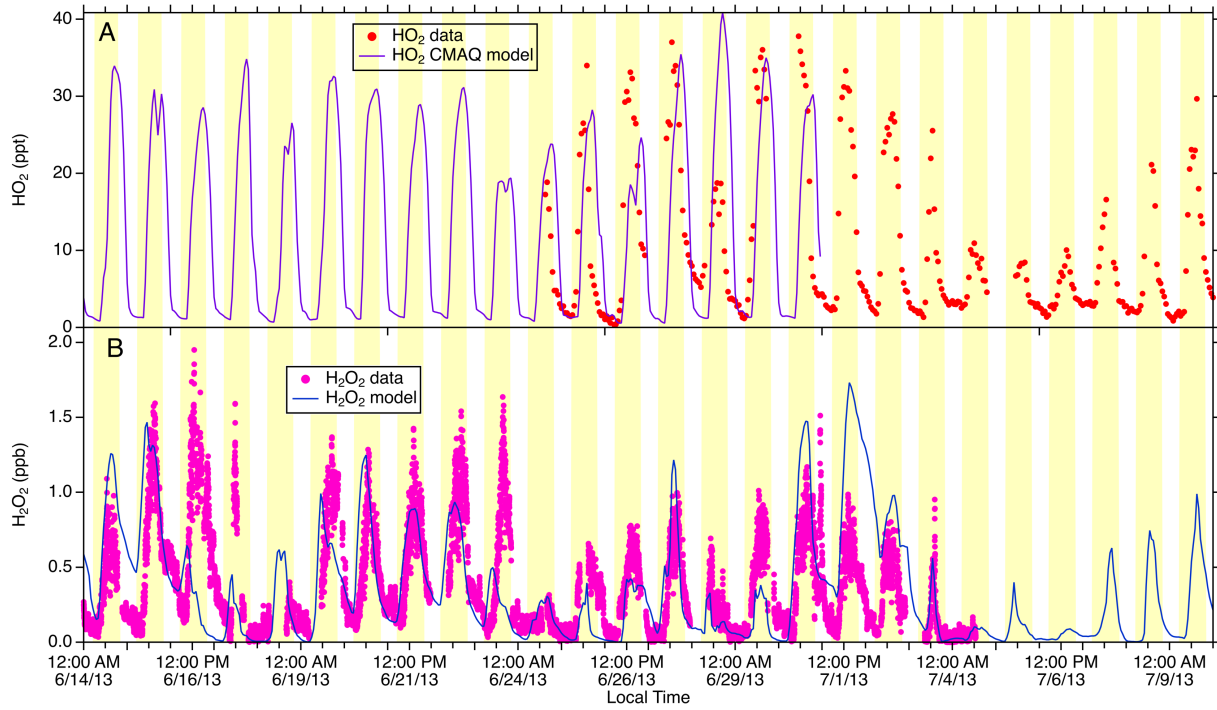
Figure S11. The time series of (A) measured and CMAQ modelled HO_2, (B) measured and

modeled H_2O_2 concentrations for the SOAS field campaign.

188
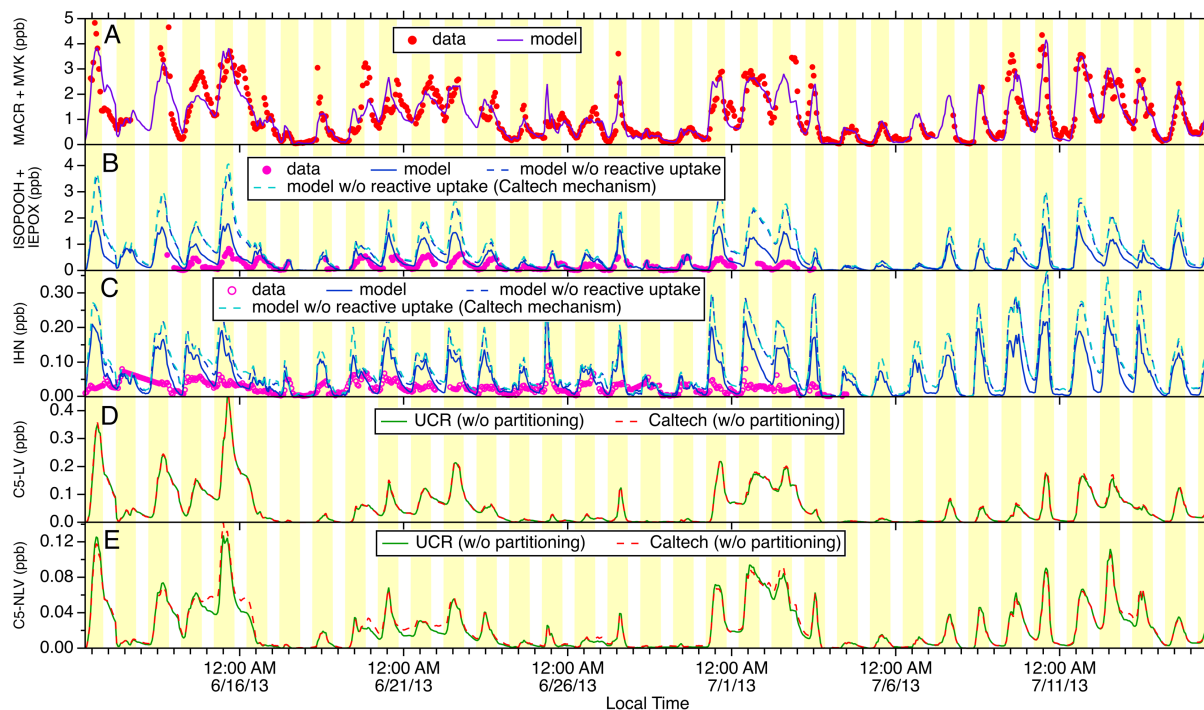
Figure S12. The time series of (A) measured and modeled MVK+MACR using UCR-ISOP; (B) measured and modeled IEPOX+ISOPOOH using both the UCR-ISOP and Caltech mechanisms, wherein for the UCR-ISOP simulations, the scenario considering IEPOX reactive uptake is also shown; (C) measured and modeled IHN using both the UCR-ISOP and Caltech mechanisms, wherein for the UCR-ISOP simulations, the scenario considering 1,2-IHN reactive uptake is also shown; (D) modeled C5-LV; and (E) modeled C5-NLV. The comparative gas-phase simulations between the UCR-ISOP and Caltech mechanisms suggest that the measurement-model disagreement is not due to any specific mechanism, but rather a lack of understanding of processes.

197

198
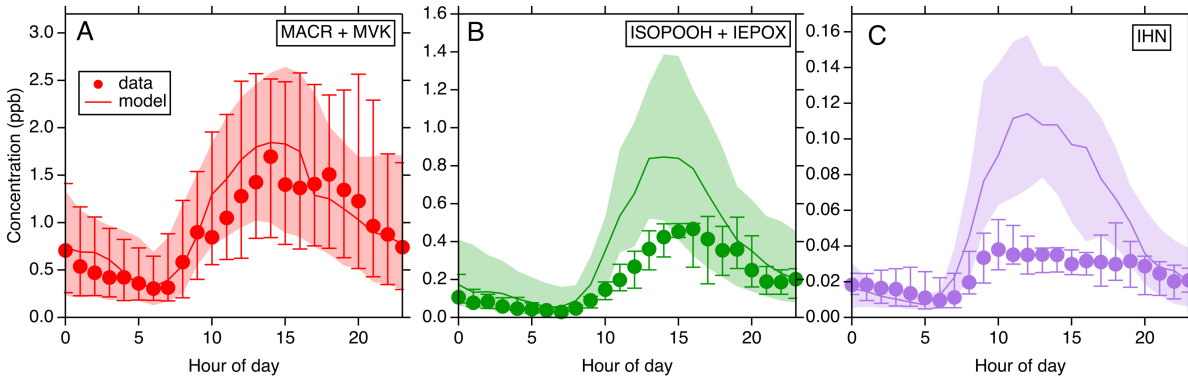
Figure S13. Measurement-simulation comparisons of the diurnal variations for (A) MACR + MVK; (B) ISOPOOH + IEPOX; and (C) IHN. The error bars represent the 25th and 75th percentiles of the measurements and the shaded areas represent the 25th and 75th percentiles of the simulations. The simulations exhibit very good agreement for measured MACR + MVK (A), but over predict ISOPOOH + IEPOX by a factor of ~ 1.8 and IHN by a factor of 1.9 (average of median values).

204
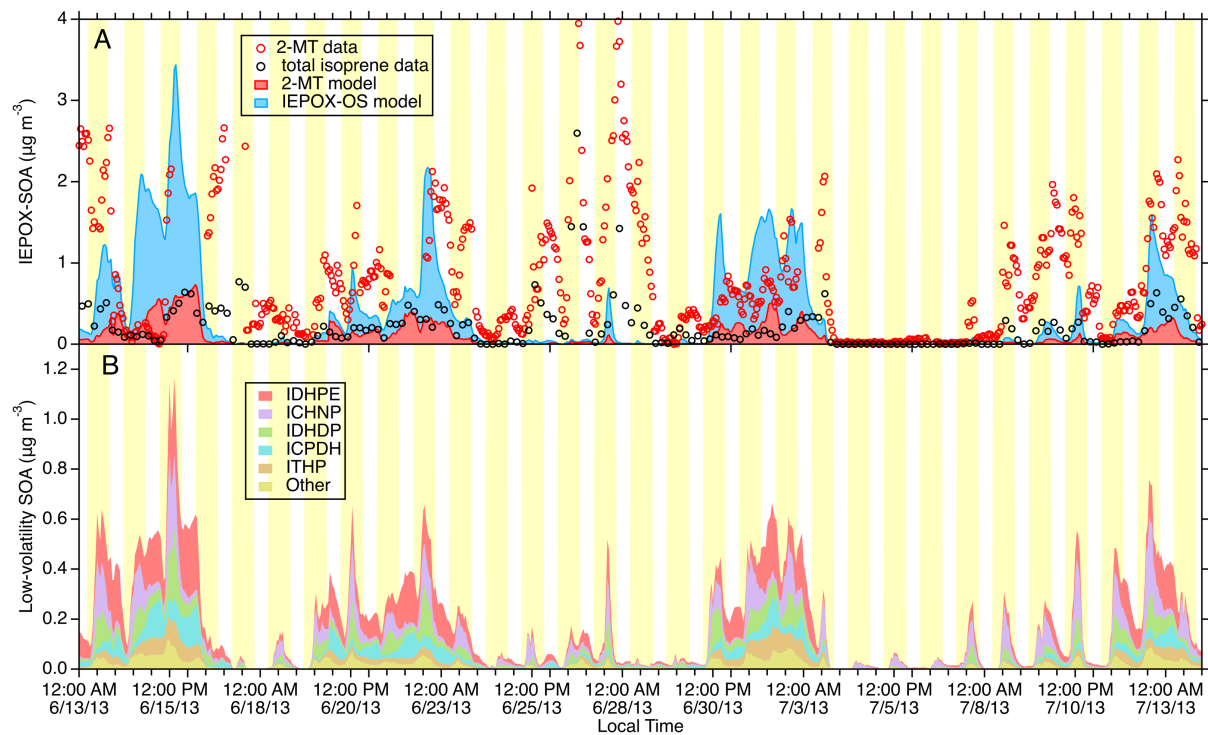
Figure S14. The time series of (A) measured (by FIGAERO-CIMS and GC×GC-MS) and modelled IEPOX-derived SOA using the UCR-ISOP mechanism and (B) modelled isoprene SOA from the low-volatility pathways.

208
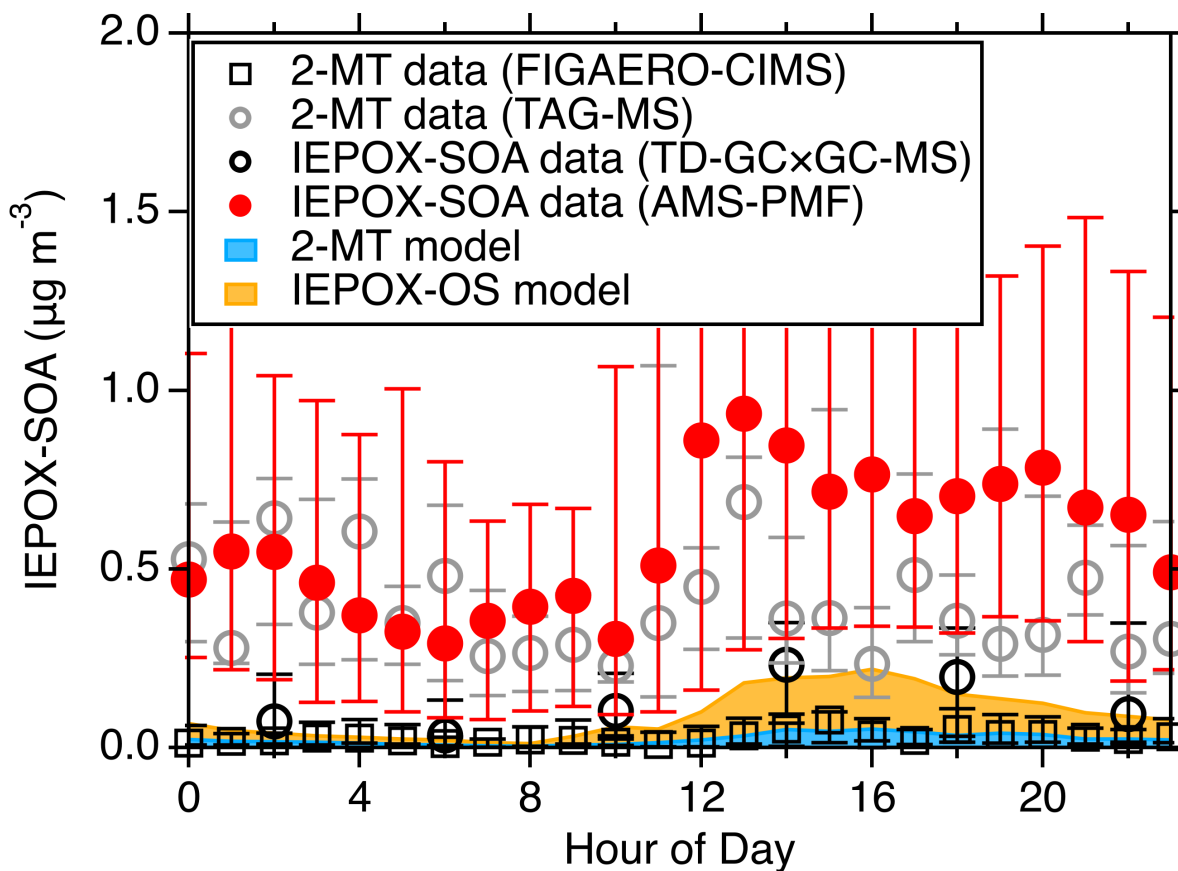
Figure S15. The diurnal trend of IEPOX-SOA comparison between the measurements and simulations, reproduced from Fig. 5A, but including the TAG-MS measurements and the IEPOX-SOA factor from AMS-PMF analysis.
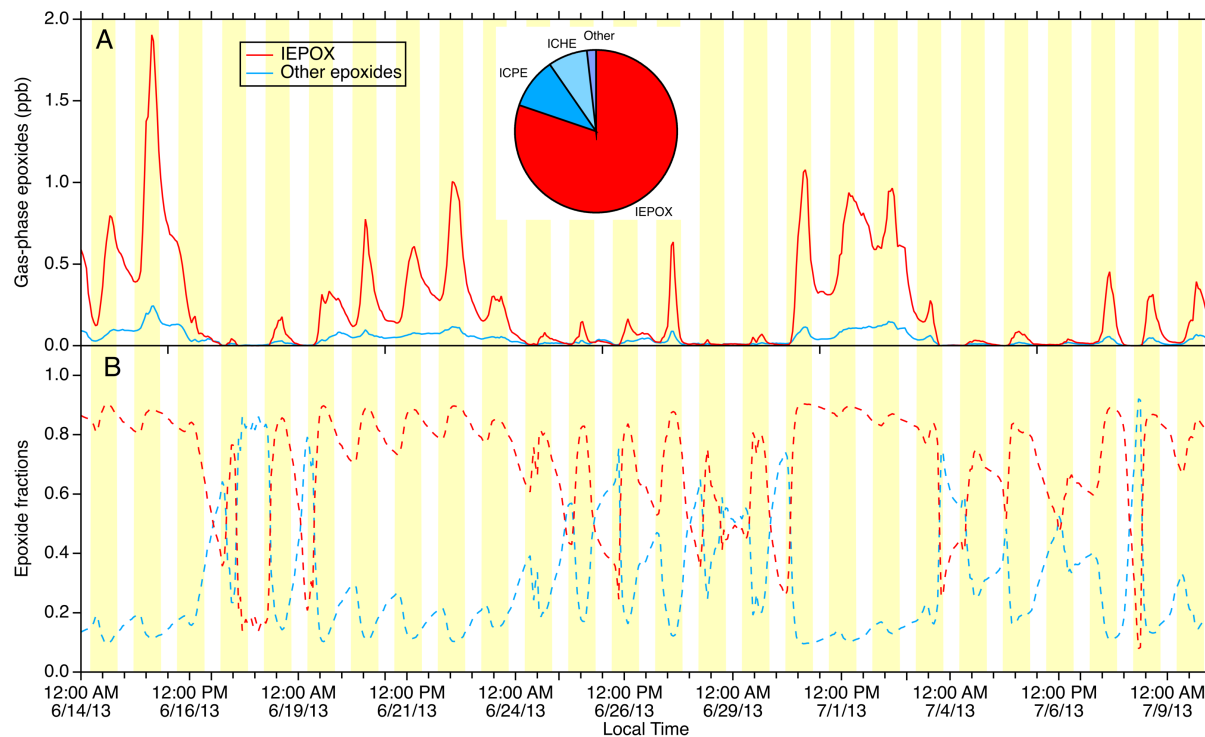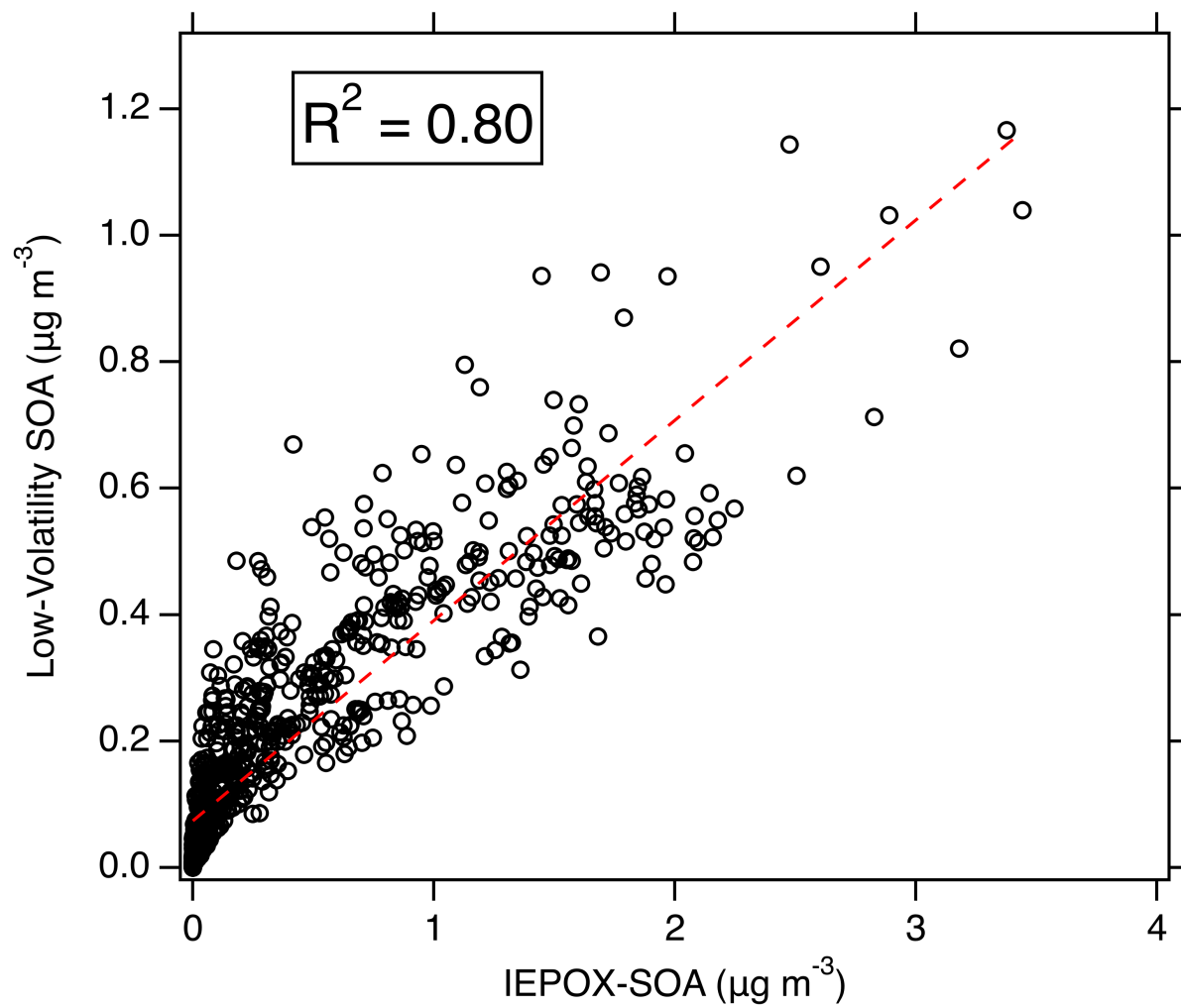
Figure S16. The time series of model predicted IEPOX and summed other epoxides for (A) concentrations and (B) relative fractions. Note, IEPOX is the sum of both β- and δ-IEPOX; the summed other epoxides do not in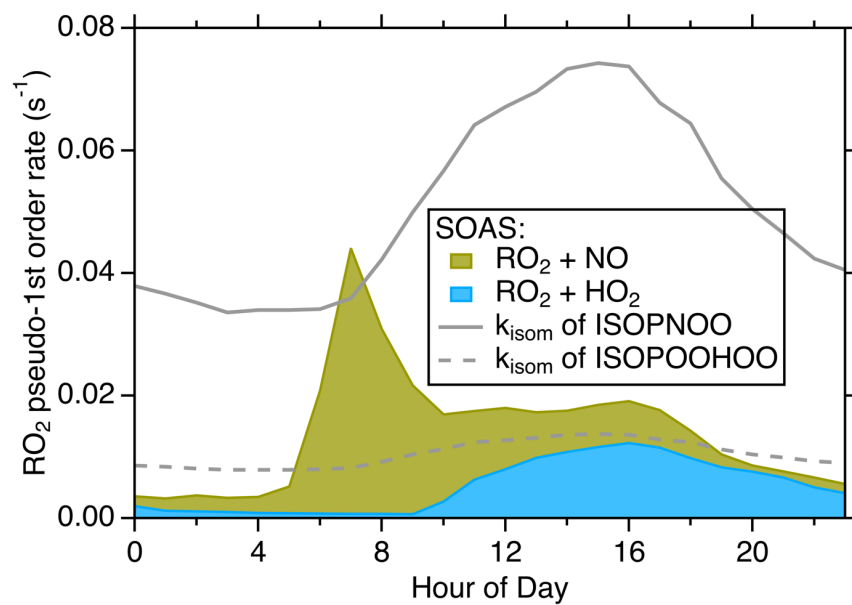clude IDHPE, which is considered a C5-LV species. The insert pie chart shows the contributions of major epoxides for SOAS medians, where IEPOX account for 80%.

218

219

Figure S17. The correlation between the simulated SOA from IEPOX reactive uptake and those

from low-volatility species (C5-LV + C5-NLV).

222

Figure S18. Pseudo-first order rates for RO_2 bimolecular reactions with NO and HO_2 during

224   SOAS, in comparison with the unimolecular isomerization rate constants for ISOPNOO and

225   ISOPOOHOO.

References

226
227
228 Kamens, R. M., Zhang, H., Chen, E. H., Zhou, Y., Parikh, H. M., Wilson, R. L., Galloway, K. E.,
229 and Rosen, E. P.: Secondary organic aerosol formation from toluene in an atmospheric
230 hydrocarbon mixture: Water and particle seed effects, Atmospheric Environment, 45, 2324-2334,
231 2011.
232 Schmedding, R., Rasool, Q. Z., Zhang, Y., Pye, H. O. T., Zhang, H., Chen, Y., Surratt, J. D.,
233 Lopez-Hilfiker, F. D., Thornton, J. A., Goldstein, A. H., and Vizuete, W.: Predicting secondary
234 organic aerosol phase state and viscosity and its effect on multiphase chemistry in a regional-scale
235 air quality model, Atmos. Chem. Phys., 20, 8201-8225, 10.5194/acp-20-8201-2020, 2020.
236 Schwantes, R. H., Teng, A. P., Nguyen, T. B., Coggon, M. M., Crounse, J. D., St. Clair, J. M.,
237 Zhang, X., Schilling, K. A., Seinfeld, J. H., and Wennberg, P. O.: Isoprene NO3 Oxidation
238 Products from the RO2 + HO2 Pathway, The Journal of Physical Chemistry A, 119, 10158-10171,
239 10.1021/acs.jpca.5b06355, 2015.
240 Thornton, J. A., Shilling, J. E., Shrivastava, M., D'Ambro, E. L., Zawadowicz, M. A., and Liu, J.:
241 A Near-Explicit Mechanistic Evaluation of Isoprene Photochemical Secondary Organic Aerosol
242 Formation and Evolution: Simulations of Multiple Chamber Experiments with and without Added
243 NOx, ACS Earth and Space Chemistry, 4, 1161-1181, 10.1021/acsearthspacechem.0c00118, 2020.
244 Zhang, H., Parikh, H. M., Bapat, J., Lin, Y.-H., Surratt, J. D., and Kamens, R. M.: Modelling of
245 secondary organic aerosol formation from isoprene photooxidation chamber studies using different
246 approaches, Environmental Chemistry, 10, 194-209, https://doi.org/10.1071/EN13029, 2013.
247 Zhang, H., Rattanavaraha, W., Zhou, Y., Bapat, J., Rosen, E. P., Sexton, K. G., and Kamens, R.
248 M.: A new gas-phase condensed mechanism of isoprene-NOx photooxidation, Atmospheric
249 Environment, 45, 4507-4521, https://doi.org/10.1016/j.atmosenv.2011.04.011, 2011.
250 Zhang, X., Cappa, C. D., Jathar, S. H., McVay, R. C., Ensberg, J. J., Kleeman, M. J., and Seinfeld,
251 J. H.: Influence of vapor wall loss in laboratory chambers on yields of secondary organic aerosol,
252 Proceedings of the National Academy of Sciences, 111, 5802-5807, doi:10.1073/pnas.1404727111,
253 2014.
254